Journal of Crystal Growth 603 (2023) 127036

Contents lists available at ScienceDirect

Journal of Crystal Growth

journal homepage: www.elsevier.com/locate/jcrysgro

Large-area 2D selective area growth for photonic crystal surface emitting lasers

Xingyu Zhao [a,1], Adam F. McKenzie [a,1,*], Connor W. Munro [a], Katherine J. Hill [a], Daehyun Kim [a], Sam L. Bayliss [a], Neil D. Gerrard [b], Donald A. MacLaren [c], Richard A. Hogg [a,b]

[a] James Watt School of Engineering, University of Glasgow, Glasgow G12 8QQ, United Kingdom
[b] III-V Epi Ltd., Glasgow G12 8QQ, United Kingdom
[c] SUPA, School of Physics and Astronomy, University of Glasgow, Glasgow G12 8QQ, United Kingdom

ARTICLE INFO

Communicated by Markus Weyers

Keywords:
A1. Characterisation
A1. Nanostructures
A3. Metalorganic vapour phase epitaxy
A3. Selective epitaxy
B2. Semiconducting III–V materials
B3. Photonic crystal surface emitting lasers

ABSTRACT

We report an investigation into large-area selective area growth of InGaAs/GaAs quantum wells by metalorganic vapour phase epitaxy. The emission wavelength tuning range, growth enhancement, and uniformity of material deposited within square masked regions with central square growth windows with widths in the range of 100–300 μm are studied. Micro-photoluminescence measurements at the centre point of each of the growth windows reveals a total wavelength tuning range of 86 nm across all samples, with a typical tuning range of 30 nm for a given window width, dependent upon dielectric mask width. The thickness enhancement in each of features, as determined by white-light interferometric profiling, indicates that centre point growth rate enhancements of between 1.19 and 2.23× are achieved with respect to the nominal epitaxial structure. By comparing the observed emission wavelengths with those simulated using the enhanced quantum well thicknesses, a range of indium concentrations between 12 and 17 % is calculated for the material at the centre of each feature. Two-dimensional analysis of selected features reveals that areas with uniform emission wavelength up to $100 \times 100\ \mu m^2$ in size can be achieved for the mask patterns used, indicating suitability for future applications in the fabrication of monolithically integrated multi-wavelength photonic crystal surface emitting laser arrays.

1. Introduction

The photonic crystal surface emitting laser (PCSEL) has emerged as a new class of laser diode that offers high-power, high-beam quality surface emission across a wide range of wavelengths in the GaAs and InP materials systems and beyond [1–8]. Wavelength selectivity in PCSELs is achieved by tuning the dimensions of the photonic crystal (PC) grating layer that is integrated epitaxially within the device next to the active region, and which supports large-area 2D coherent laser oscillation and surface emission through second-order Bragg scattering [9]. Owing to their attractive characteristics, PCSELs have been identified as ideal candidates for realising surface emitting laser arrays, with previous work in this regard having demonstrated coherent coupling and power scaling in single-wavelength arrays [10–12]. The ability to realise a monolithically integrated mulitcolour array, whereby devices fabricated on the same substrate emit over a range of wavelengths, would signify an important step in the development of PCSEL technology, allowing their use in wavelength division multiplexing and sensing applications which require a multi-wavelength source.

Recently, the monolithic fabrication of PCSELs at four different wavelengths was demonstrated in InP-based materials, with room-temperature continuous-wave lasing across a 40 nm wavelength range from 1300 to 1340 nm being reported [13]. The wavelength tuning was achieved using a common active material by varying the period of the PC grating to accommodate four separate lasing modes across a single gain band. Whilst, in principle, the cavity mode of a PC can be designed to span more than 100 nm for a given system [9], the range of wavelengths accessible to a monolithic array realised in this manner is expected to be limited to less than 50 nm, due to the limited gain bandwidth of MQW active regions and the deleterious effects on device performance associated with a large detuning of the lasing mode (i.e. PC mode) from the gain peak for the active region.

A common way of expanding the wavelength range available to multicolour laser arrays is to spatially vary the composition of the gain

* Corresponding author.
E-mail address: Adam.McKenzie@glasgow.ac.uk (A.F. McKenzie).
[1] These authors contributed equally to this work.

https://doi.org/10.1016/j.jcrysgro.2022.127036
Received 13 October 2022; Received in revised form 5 December 2022; Accepted 6 December 2022
Available online 13 December 2022
0022-0248/© 2022 The Authors. Published by Elsevier B.V. This is an open access article under the CC BY license (http://creativecommons.org/licenses/by/4.0/).

material on the wafer. Traditionally, this has been achieved by selective area growth (SAG) of multi-quantum well (MQW) laser structures on wafers which have been pre-patterned with a series of growth windows enclosed by areas of dielectric material [14]. The presence of an amorphous dielectric (such as SiO_2) on the surface of the wafer acts as a mask, preventing deposition of the *epi* layers on those regions. As a result, there is a net diffusion of material into the adjacent growth windows leading to an enhancement of the growth rate and thickness of the MQW stack, as well as a variation in alloy composition across the window. Consequently, the emission wavelength of the material is shifted with respect to the nominal structure, the extent to which can be tuned considerably by varying the relative widths of the SAG window and mask [15]. By exploiting this principle, multi-channel laser arrays with wavelength ranges spanning up to 150 nm have been successfully fabricated in the past [16,17], highlighting the potential for significantly expanding the wavelength range available to monolithic PCSEL arrays.

In the context of application of SAG to PCSELs, two key challenges can be identified; the 2D nature of the devices (i.e., the requirement for a 2D PC grating layer), and the large device area required for efficient operation, which is generally considered to be greater than 100 × 100 μm^2 [9]. To date, the development of conventional MQW SAG technology has been focused almost exclusively on devices with one dimensional (1D) geometries, such as buried-heterostructure lasers [16,18], integrated laser-modulator structures [19], or photonic integrated circuits [17,20]. Such devices typically require uniform gain material with a width on the order of 10–20 μm for successful fabrication of devices (at least one order of magnitude less than required for a PCSEL). Consequently, the SAG mask geometries reported in literature typically consist of window widths between 20 and 60 μm, with mask widths varying by up to as much as 10× the window width. In the case of the few examples where window widths exceeding 100 μm have been reported, data on the level of growth rate enhancement (GRE) and wavelength shift for the InGaAs/GaAs MQW system was limited to a single mask width, and no extensive study of the wavelength tuning range were reported [21–23].

This work presents, to the best of our knowledge, the first study of InGaAs/GaAs MQWs selectively grown in large area 2D SAG windows with dimensions up to 300 × 300 μm^2. Initially, point analysis at the centre of the masked features is presented, with the enhancement in QW emission wavelength and thickness elucidated in each case through room-temperature μ-photoluminescence (μ-PL) measurements and white-light interferometry (WLI) profiling, respectively. The variation in indium concentration with respect to the nominal QW structure is then determined for all features by comparison of calculated and observed emission wavelengths. Following this, for selected features, the initial point analysis is extended to the entirety of the 2D SAG area by further μ-PL mapping, allowing regions of uniform material with areas up to 100 × 100 μm^2 to be identified.

2. Sample preparation and measurement

A five-by-five array of square SAG regions were defined on *epi*-ready *n*-GaAs substrates orientated with a 2°-offcut from the (100) plane towards $(1\bar{1}0)$. Following deposition of a 200 nm-thick SiO_2 layer on the surface of the wafer, masked regions were defined by conventional lithography and inductively coupled plasma etching, with edges aligned along the {110} crystal plane directions. The widths of the SiO_2 masks, W and the open SAG windows, Λ were varied from 100 to 300 μm, in 50 μm increments, giving 25 regions with unique W and Λ combinations. A schematic of the mask layout is shown in Fig. 1(a). The centre-to-centre distance between SAG windows was set at 2 mm in order to prevent vapour-phase interference between neighbouring regions [24], and the total dielectric coverage on the wafer was approximately 8.5 %.

The epitaxial structure was deposited by metalorganic vapour phase epitaxy (MOVPE) in a Thomas Swan closed-coupled showerhead reactor

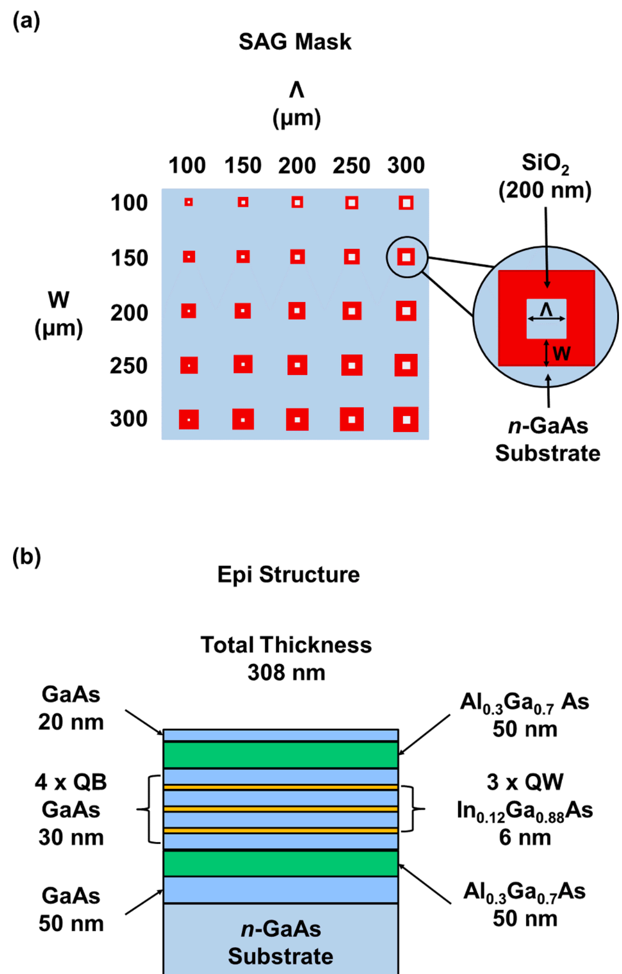

Fig. 1. (a) Plan-view schematic showing the layout of SAG regions. Features form a 5 × 5 array with centre-to-centre distance of 2 mm. The window width, Λ and SiO2 mask width, W vary between 100 and 300 μm. (b) Cross-sectional schematic of the nominal *epi* structure studied. The MQW structure consists of three 6 nm-thick $In_{0.12}Ga_{0.88}As$ QWs, tuned to emit at 945 nm, separated by 30 nm GaAs barriers. The nominal thickness of deposited material in un-masked regions is 308 nm.

utilising trimethylaluminium (TMAl), trimethylgallium (TMGa), trimethylindium (TMIn), and arsine (AsH_3) as precursors. The undoped structure consisted of three 6 nm-tick $In_{0.12}Ga_{0.88}As$ QWs tuned to emit at 945 nm in the field far from the SAG mask, and four 30 nm-thick GaAs barriers. The MQWs were confined between two 50 nm-thick $Al_{0.30}Ga_{0.70}As$ layers to help with carrier confinement and room-temperature PL intensity, and 50 nm and 20 nm-thick GaAs buffer and capping layers. A cross-sectional schematic is shown in Fig. 1(b). The entire structure was grown at a temperature of 650 °C and pressure of 100 mbar, with the growth rate and V/III ratio for InGaAs growth set at 23 nm/min and 300, respectively. Growth conditions were chosen to minimise polycrystalline deposition on the large, masked areas, whilst ensuring high-quality material in the field far from the oxide mask [22].

The shift in QW emission wavelength at the centre of each of the SAG features was determined by μ-PL measurements made at a temperature of 298 K. Excitation was achieved using a 532 nm green laser focused to a spot on the wafer surface approximately 10 μm in diameter. The spot size (which is the smallest possible for the system used) was chosen to limit the potential spectral broadening associated with anisotropic material and to allow for reasonable spatial resolution and sampling size during 2D mapping, for which the step size was also set at 10 μm. The resolution of the spectrometer used was 0.5 nm, giving an uncertainty in

peak wavelength of ±1 nm; this value is used as the acceptance condition when defining the uniformity of material in the final stage of the 2D analysis. The thickness of the selectively grown material was determined by WLI measurements using a Bruker Contour Optical Profilometer. The vertical resolution of measurements is approximately 5 nm. Prior to measurements, the SiO_2 mask was removed from the sample surface using a 10:1 buffered HF wet etch solution to provide access to the original wafer surface as a reference point. Whilst the composition of epitaxially grown material can usually be determined using X-ray diffraction measurements, the spot size and spatial resolution required of the analysis of selectively grown material is more than an order of magnitude smaller than that available in lab-based diffractometers [25]. In the absence of high-resolution facilities, the indium concentration of the materials described here were determined by comparing the measured QW emission wavelengths with those calculated using LaserMod simulation software, with the measured emission wavelengths and QW thicknesses used as input parameters.

3. Results and discussion

In order to determine the range of emission wavelength shifts and GREs that can be realised using large area SAG features, point analysis was initially conducted at each of the 25 growth sites. The emission wavelengths of the selectively grown MQW material were measured at the centre point of the SAG windows at room temperature. Representative PL spectra for three features with window width, Λ = 200 μm and mask widths, W = 200, 250, and 300 μm are shown in Fig. 2(a). In each case, the measured wavelength is longer than the 945 nm emission of the nominal *epi* structure in the field far from the SAG mask, and increases from 985 nm (orange) to 991 nm (blue) and 994 nm (green) with increasing mask width. During SAG, the low surface reaction rate on SiO_2 prevents deposition of material on the masked areas of the wafer, creating the situation where a large concentration gradient exists normal to the surface of the exposed window region as reactants are consumed, whilst there is effectively zero gradient above the masked region [26]. Consequently, reactant species in the boundary layer above the mask preferentially diffuse in the gas-phase towards the SAG window and deposit there, resulting in a GRE within the window with respect the nominal planar growth rate. The observed red-shift in peak wavelength described here is in line with an enhanced QW thickness resulting from such a GRE. As the mask width increases, a larger gradient in reactant concentration is established above the SAG window, driving a larger GRE [27]. The spectra, which are broadly representative of those collected from all growth sites, display narrow full-width-half-maximum (FWHM) values between 14 and 19 nm indicating that the material at the centre of each of the features is of good-quality and suggesting that there has been little degradation of the interfaces between the layers of the MQW structure.

The central peak emission wavelengths from all SAG features are shown in Fig. 2(b), plotted as a function of both W and Λ. In all cases, the measured wavelength is longer 945 nm, indicating that a GRE is present even for the largest of the window widths. The red-shift is smallest for the SAG regions with Λ = 300 μm and W = 100 μm which exhibits 954 nm emission, and largest for Λ = 100 μm and W = 300 μm, where emission is at 1031 nm. This represents a total wavelength tuning range of 86 nm across the wafer, relative to the nominal MQW structure in the unmasked region. Two trends are observed with regards to the extent of the shift. Firstly, for a given mask width, W the emission wavelength increases with decreasing window width, Λ. Second, for a given window width, wavelength increases with increasing mask width. Both of these trends are consistent with the larger GRE expected for increasing values of mask-to-window width ratio (W/Λ), and the larger concentration gradients that result [28]. Considering the latter trend, the wavelength tuning ranges for individual mask widths lie between 26 and 46 nm. Whilst modest, tuning ranges on this order are broadly comparable with those reported in the literature for InGaAs/GaAs QW SAG when the

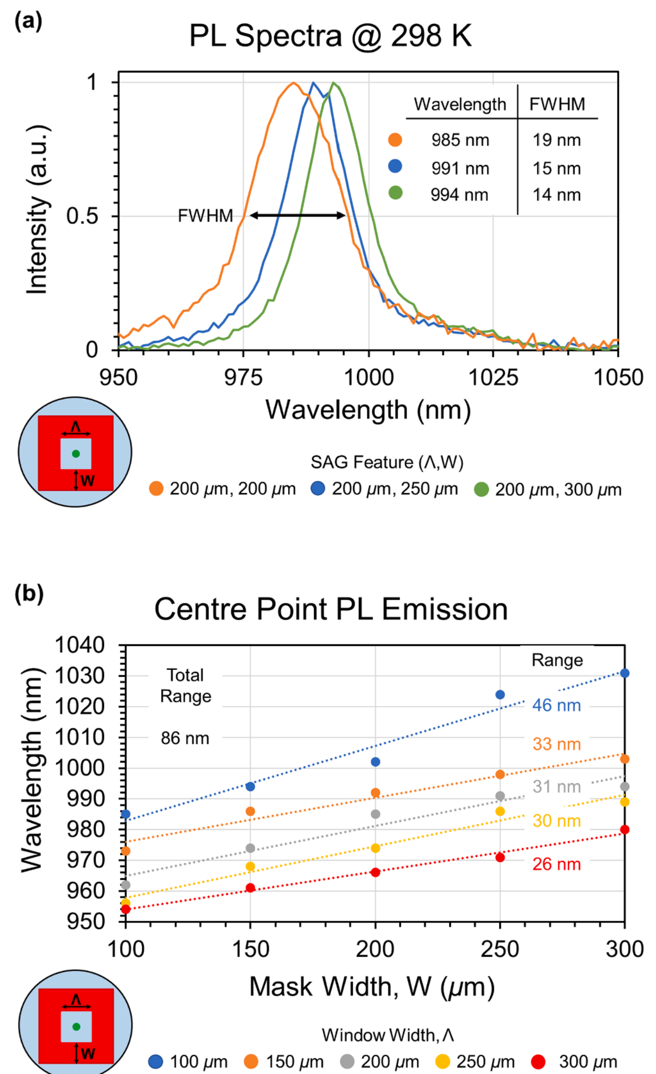

Fig. 2. (a) Room-temperature PL spectra from the centre point of three SAG features with a common window width, Λ = 200 μm and mask widths, W = 200 μm (orange), 250 μm (blue), 300 μm (green). (b) Peak room-temperature PL emission wavelength at the centre point of each SAG feature. A wavelength tuning range of 86 nm is achieved across all features relative to the nominal 945 nm emission of the material in the field far from the SAG mask. Straight lines are included as an aid for the eyes.

small ratios of W/Λ used in our case (0.33 ≤ W/Λ ≤ 3) are considered [22,29].

In order to determine the extent of the GRE associated with the large SAG feature dimensions, the thickness profiles of the deposited material within the windows were mapped using WLI profiling. Representative line profiles taken along the x direction of three features with window width, Λ = 200 μm and mask widths, W = 200, 250, and 300 μm are shown in Fig. 3(a). The thickness values are given in terms of an enhancement factor, which is simply the ratio of the measured thickness of the entire structure to the nominal 308 nm thickness for the as-grown material. The observed profiles are characteristic of those obtained during SAG, with the lateral gradients in reactant concentrations installed across the window region giving rise to a concave profile, with the GRE being largest directly adjacent to the dielectric mask and decreasing towards the centre of the window [26]. The centre point enhancement factors for these features lie between 1.5 and 1.9×, with the value increasing with increasing mask width, in line with previously reported trends [18]. The thickness profile along the y direction of the windows are nominally identical to those of the x scan in both shape and

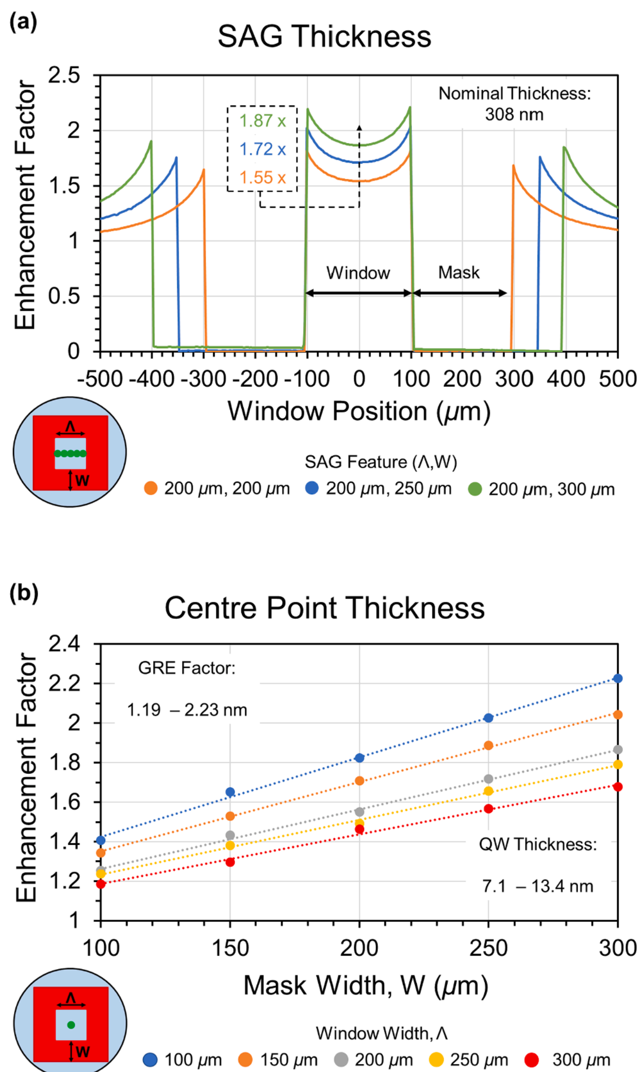

Fig. 3. (a) Thickness profiles of three SAG features with a common window width, Λ = 200 μm and mask widths, W = 200 μm (orange), 250 μm (blue), 300 μm (green), as determined by WLI profiling. (b) Thickness values are presented as enhancement factors relative to the nominal *epi* thickness of 308 nm. Measured growth rate enhancement factors at the centre point of each of the SAG features. A range of enhancement factors from 1.19 to 2.23 × are observed, corresponding to QW thicknesses of 7.1–13.4 nm. Straight lines are included as an aid for the eyes.

magnitude of the recorded enhancement factors, suggesting that any anisotropy in growth kinetics associated with alignment of the SAG mask along orthogonal crystal plane directions are minimal over the large distances employed here. Centre point GRE factors from all SAG features are shown in Fig. 3(b), plotted as a function of both W and Λ. As with the shift in emission wavelength described above, the thickness of the selectively grown material increases with increasing W/Λ, with enhancement factors spanning a range from 1.19 to 2.23× the nominal thickness, values that are typical of those obtained during SAG of InGaAs/GaAs structures [18]. As GaAs is the dominant constituent component, the deposited *epi* layers (high gallium concentration alloys $In_{0.12}Ga_{0.88}As$ and $Al_{0.30}Ga_{0.70}As$ were used), and gallium has the longest vapour phase diffusion length of the group-III species, it is assumed that the thickness of the individual layers are uniformly enhanced [20,24]. Consequently, a corresponding range of modified QW thicknesses from 7.1 nm to 13.4 nm is obtained.

The extent to which the observed shifts in PL wavelength are driven by the GRE was determined by simulations of the emission wavelength expected for $In_{0.12}Ga_{0.88}As$/GaAs QWs with the enhanced thicknesses measured above. The calculated wavelengths are shown in Fig. 4(a). As expected, the increased QW thickness results in a lengthening of the emission wavelength relative to the nominal structure. However, the degree of red-shifting is significantly truncated compared to the measured centre point wavelengths described in Fig. 2(b), with the total tuning range for the calculated values being only 32 nm compared with the 86 nm observed in reality. The difference in the calculated and observed wavelength increased significantly as the W/Λ ratio of the features increases. For the smallest values of W/Λ (Λ = 300 μm, W = 100 μm and Λ = 250 μm, W = 100 μm) the wavelengths differ by less than 1 nm, whilst for largest W/Λ features (Λ = 100 μm, W = 250, 300 μm) the enhanced QW thickness accounts for only 38 % of the observed red-shift. Consequently, a higher indium concentration is required in the QW to completely account for the measured wavelength enhancement, and the required indium mole fraction increases significantly compared to the nominal 12 % value as the W/Λ ratio of the SAG features

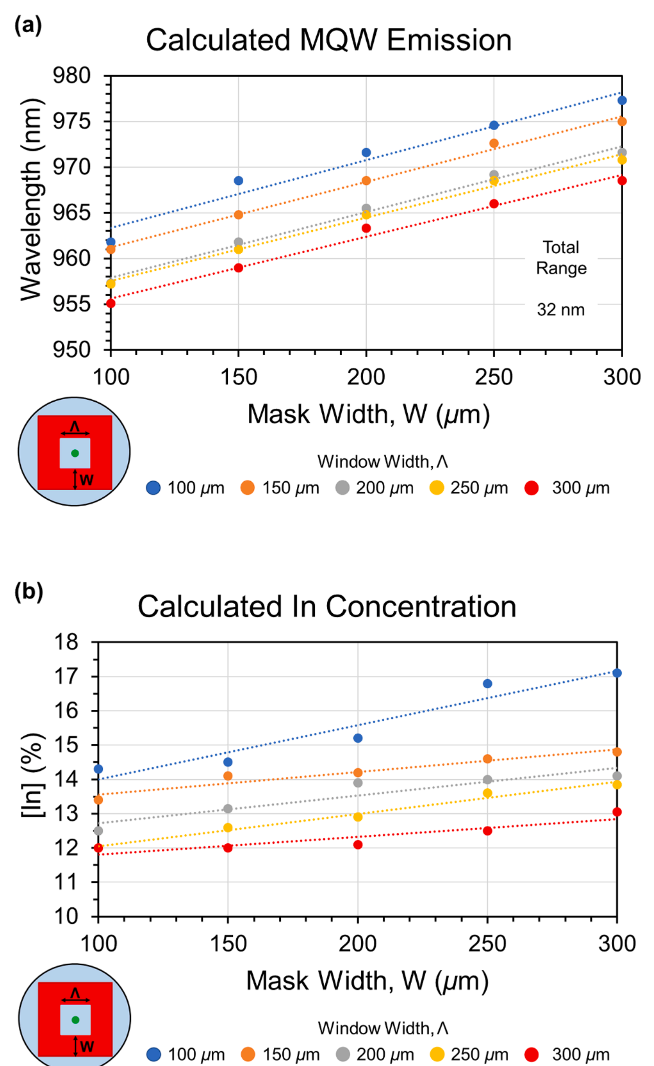

Fig. 4. (a) Calculated emission wavelengths of $In_{0.12}Ga_{0.88}As$ quantum wells simulated using only the enhanced thickness values determined by WLI profiling. A large difference between calculated values and those observed in PL measurements of the selectively grown material. (b) Calculated indium concentration at the centre of each SAG feature. Values were determined by simulation of InGaAs QW with enhanced thicknesses, determined above. The indium concentrations are those required to obtain the same wavelength observed in centre point PL measurements. Straight lines are included as an aid for the eyes.

increases. The necessary concentration at the centre-point of the SAG masks were determined by modifying the above simulations to account for an indium variation such that the emission wavelengths match those measured by PL. The calculated indium concentrations are shown in Fig. 4(b), plotted as a function of both W and Λ. For the features with the smallest W/Λ ratio, the concentration is virtually unchanged from the nominal 12 % value, confirming that wavelength shift in this case is derived almost entirely from the QW thickness enhancement. As indicated by the trends in Fig. 4(a), the indium percentage increases significantly to 17 % for the features with the largest W/Λ ratio, where it accounts for a larger fraction of the observed red-shift. An enhanced QW indium mole fraction is expected for these features owing to the relative increase in the gas-phase reactant concentration associated with large masked areas, which gives rise to a larger concentration gradient between the mask and window regions [20,27,28].

For selected features, the point analysis performed above was extended to cover the entire growth window in order to assess the uniformity of the selectively grown material. A representative 2D μ-PL map for the SAG feature with Λ = 200 μm, W = 250 μm is shown in Fig. 5. The wavelength distribution across the window is characterised by a large central area in which the wavelength is relatively uniform, surrounded by concentric regions of material with longer wavelengths, increasing significantly towards the edge of the dielectric mask. This distribution is equivalent to that seen for conventional 1D SAG and is explained by the lateral concentration gradients that are established above the growth window [27,28]. In addition to the concave thickness profile discussed previously, the concentration gradient gives rise to an anisotropy in the indium mole fraction across the window. Reactive indium-species exhibit much shorter gas-phase diffusion lengths compared with gallium, and more readily adsorb to the surface as they diffuse across the window. As a result, the relative indium concentration of the material within a few tens of microns of the mask edge is greatly enriched compared with that at the centre of the window, and the QW emission wavelength is further enhanced [20,24,26].

The wavelength and indium distributions across the window are visualised in the line scans shown in Fig. 6. As before, the indium concentration at each point (Fig. 6(c)) was calculate by QW simulations created using the enhance well thickness determined by WLI measurements (Fig. 6(b)) and the emission wavelengths extracted from the PL map (Fig. 6(a)). With regard to the variation in indium concentration, a value of 14.2 % is calculated for the material at the centre point. The

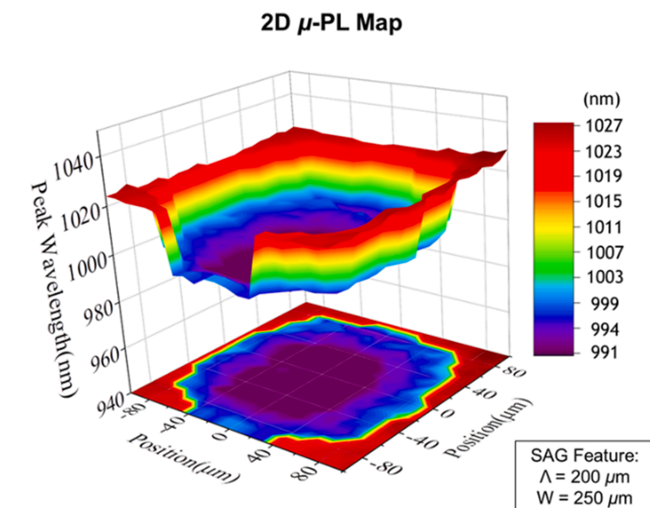

Fig. 5. 2D μ-PL map for the SAG feature with Λ = 200 μm and W = 250 μm. The wavelength distribution across the growth window is concave, with the wavelength increasing concentrically from the centre point to the edge of the dielectric mask. A large region of material with uniform emission wavelength is observed at the centre of the window.

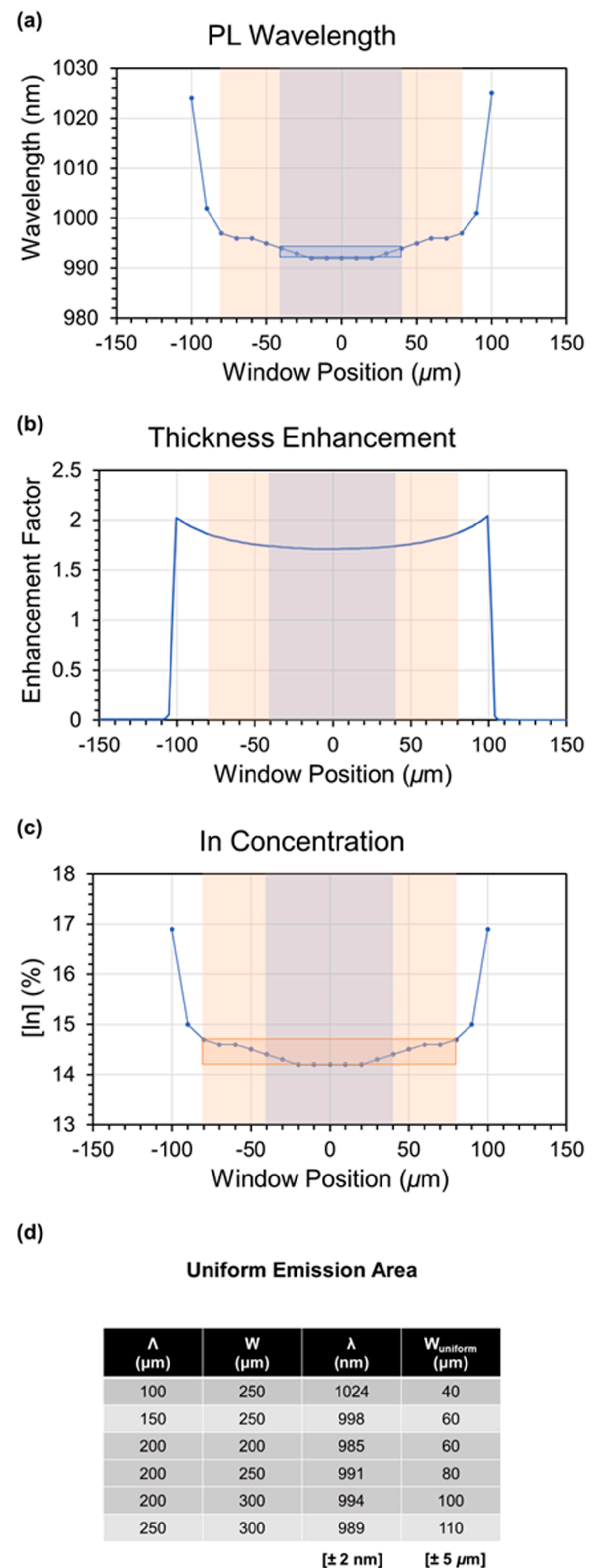

Λ (μm)	W (μm)	λ (nm)	$W_{uniform}$ (μm)
100	250	1024	40
150	250	998	60
200	200	985	60
200	250	991	80
200	300	994	100
250	300	989	110
		[± 2 nm]	[± 5 μm]

Fig. 6. Extended 2D analysis for feature with Λ = 200 μm and W = 250 μm. Line scans of the (a) emission wavelength, (b) thickness enhancement, (c) and indium concentration across the SAG window are shown. Wavelength and indium values were determined from 2D μ-PL mapping. The area with uniform emission, within 2 nm of the centre point value, is highlighted in blue. The area in which the indium concentration varies within 0.5 % is highlighted in orange. (d) Table showing the width of the uniform emission area for selected SAG features, as determined by 2D analysis. The width of the uniform area, $W_{Uniform}$ is accurate to within ±5 μm.

concentration varies within 0.5 % of this value across the majority of the growth window, covering an area of approximately 160 μm (as highlighted by the orange box). Beyond this, the indium concentration increases significantly, rising to 16.9 % at the boundary of the dielectric mask. This result suggests that the lateral concentration gradient driving the indium variation is dominated by species arriving at the window from directly above the mask for a length approximately 20 μm of its edge, and that the indium enhancement across the majority of the window is determined primarily by vapour phase diffusion of species from higher up in the boundary layer. This is in reasonable agreement with a gas phase diffusion length for indium on the order of 30 μm as determined by modelling of the AlGaInAs/InP system [20,24].

The wavelength variation across the window (Fig. 6(a)) follows a similar trend to that of the indium concentration, with a longer wavelength of 1024 nm observed at the edge of the mask compared with the 991 nm centre point, driven by the large inhomogeneity in the indium mole fraction. In defining an area in which the emission wavelength is deemed to be uniform, a constraint of ±2 nm relative to the centre point wavelength is used – this value is chosen to allow a conservative limit of ±1 nm variation on top of the ±1 nm uncertainty arising from the wavelength resolution of the PL measurement. The width of the uniform emission area (which is highlighted in blue) is determined to be approximately 80 μm, with an uncertainty of ±5 μm originating from the choice of laser spot and step size used during PL mapping. Line scans taken along the orthogonal axis of growth window show little variation in terms of measured wavelength values and calculated indium concentrations, or in the width of the uniform emission region, suggesting that growth within the large 2D windows is not significantly affected by any natural anisotropies in growth kinetics. It is noted that the total wavelength variation across the 160 μm region identified above (orange box) is limited to only 6 nm, suggesting that the area of the uniform emission can be expanded by re-evaluating the growth conditions used to enhance the diffusion of species within the window and flatten the wavelength distribution.

Similar analysis was performed for five additional features, the results of which are summarised in Fig. 6(d). In general, two trends are observed with regards to the width of the uniform emission area. Firstly, for a fixed W, the width of the area increases as Λ increases, whilst the wavelength decreases. Secondly, the for a fixed Λ, both the width of the area and the wavelength increase with W. Significantly, two features (Λ = 200 μm, W = 300 μm and Λ = 250 μm, W = 300 μm) are identified for which the uniform emission area exceeds 100 × 100 μm^2, approaching the minimum scale required for the fabrication of PCSELs. It is worth noting that in terms of operation, the gain bandwidth of the active element is expected to be much larger (>30 nm) than these values of wavelength change (±2 nm), resulting in spatially varying (de-)tuning of the laser wavelength to the gain peak. From the line-scans in 6(a) we expect lasing to be supported in the whole area of the SAG mask, with the possible exception of the approximately 20 μm wide perimeter at the boundary of the aperture and SAG mask.

4. Conclusions

We have presented a study of InGaAs/GaAs MQW structures selectively grown in large 2D SAG features. It has been shown that the thickness and compositional variation associated with SAG is effective in features with dimensions up to 300 × 300 μm^2, resulting in a total wavelength tuning range of 86 nm across all growth sites, with respect to the respect to the nominal *epi* structure. For a given window width, the degree of red-shifting increases with dielectric mask width, producing a typical tuning range on the order of 30 nm. For features with the largest W/Λ ratio, the wavelength shift is dominated by a greatly enhanced QW indium mole fraction up to 17 % at the centre of the growth window, whilst the indium concentration varies little from the nominal 12 % where W/Λ is small. 2D analysis reveals that the wavelength distribution across the growth windows is characterised by a large central region in which the emission wavelength is uniform within 2 nm. Isotropic regions with areas up to 100 × 100 μm^2 have been achieved, indicating that SAG may be a suitable technique for the realisation of monolithic multicolour PCSEL arrays in the future.

CRediT authorship contribution statement

Xingyu Zhao: Methodology, Formal analysis, Investigation. **Adam F. McKenzie:** Methodology, Formal analysis, Investigation, Writing – original draft, Writing – review & editing. **Connor W. Munro:** Investigation. **Katherine J. Hill:** Methodology, Investigation. **Daehyun Kim:** Investigation. **Sam L. Bayliss:** Investigation. **Neil D. Gerrard:** Methodology, Investigation. **Donald A. MacLaren:** Writing – review & editing, Supervision. **Richard A. Hogg:** Resources, Writing – review & editing, Supervision.

Declaration of Competing Interest

The authors declare that they have no known competing financial interests or personal relationships that could have appeared to influence the work reported in this paper.

Data availability

Data will be made available on request.

Acknowledgements

A.F.M. is grateful for the support of the Royal Commission for the Exhibition of 1851 through an Industrial Fellowship.

References

[1] T.-C. Lu, S.-W. Chen, T.-T. Kao, T.-W. Liu, Characteristics of GaN-based photonic crystal surface emitting lasers, Appl. Phys. Lett. 93 (11) (2008) 111111.
[2] R.J.E. Taylor, D.M. Williams, J.R. Orchard, D.T.D. Childs, S. Khamas, R.A. Hogg, Band structure and waveguide modelling of epitaxially regrown photonic crystal surface-emitting lasers, J. Phys. D Appl. Phys. 46 (26) (2013) 264005.
[3] K. Hirose, Y. Liang, Y. Kurosaka, A. Watanabe, T. Sugiyama, S. Noda, Watt-class high-power, high-beam-quality photonic-crystal lasers, Nature Photon. 8 (5) (2014) 406–411.
[4] M. Yoshida, M. De Zoysa, K. Ishizaki, Y. Tanaka, M. Kawasaki, R. Hatsuda, B. Song, J. Gelleta, S. Noda, Double-lattice photonic-crystal resonators enabling high-brightness semiconductor lasers with symmetric narrow-divergence beams, Nature Mater. 18 (2) (2019) 121–128.
[5] Z. Bian, K.J. Rae, A.F. McKenzie, B.C. King, N. Babazadeh, G. Li, J.R. Orchard, N. D. Gerrar, S. Thoms, D.A. MacLaren, R.J.E. Taylor, D.T.D. Childs, R.A. Hogg, 1.5 μm epitaxially regrown photonic crystal surface emitting laser diode, IEEE Photon. Technol. Lett. 22 (24) (2020) 1531.
[6] A.F. McKenzie, B.C. King, K.J. Rae, S. Thoms, N.D. Gerrard, J.R. Orchard, K. Nishi, K. Takemasa, M. Sugawara, R.J.E. Taylor, D.T.D. Childs, D.A. MacLaren, R. A. Hogg, Void engineering in epitaxially regrown GaAs-based photonic crystal surface emitting lasers by grating profile design, Appl. Phys. Lett. 118 (2021), 021109.
[7] Y.-H. Huang, Z.-X. Yang, S.-L. Cheng, C.-H. Lin, G. Lin, K.-W. Sun, C.-P. Lee, Effect of hole shift on threshold characteristics of GaSb-based double-hole photonic-crystal surface-emitting lasers, Micromachines 12 (2021) 468.
[8] Y. Itoh, N. Kono, D. Inoue, N. Fujiwara, M. Ogasawara, K. Fujii, H. Yoshinaga, N. Yagi, M. Yanagisawa, M. Yoshida, T. Inoue, M. De Zoysa, K. Ishizaki, S. Noda, High-power CW oscillation of 1.3-μm wavelength InP-based photonic-crystal surface emitting lasers, Optics Express 30 (16) (2022) 29539.
[9] K. Ishizaki, M. De Zoysa, S. Noda, Progress in photonic-crystal surface-emitting lasers, Photonics 6 (2019) 96.
[10] R.J.E. Taylor, D.T.D. Childs, P. Ivanov, B.J. Stevens, N. Babazadeh, J. Sarma, S. Khamas, A.J. Crombie, G. Li, G. Ternent, S. Thoms, H. Zhou, R.A. Hogg, Coherently coupled photonic-crystal surface emitting laser array, IEEE J. Select. Topics Quant. Electron. 21 (6) (2015) 4900307.
[11] R.J.E. Taylor, D.T.D. Childs, P. Ivanov, B.J. Stevens, N. Babazadeh, A.J. Crombie, G. Ternent, S. Thoms, H. Zhou, R.A. Hogg, Electronic control of coherence in a two-dimensional array of photonic crystal surface emitting lasers, Sci. Rep. 5 (2015) 13203.
[12] B.C. King, K.J. Rae, A.F. McKenzie, A. Boldin, D.-H. Kim, N.D. Gerrard, G. Li, K. Nishi, K. Takemasa, M. Sugawara, R.J.E. Taylor, D.T.D. Childs, R.A. Hogg, Coherent power scaling in photonic crystal surface emitting laser arrays, AIP Adv. 11 (2021), 015017.

[13] C. Hill, J.R. Orchard, I. Javed, C.W. Munro, D.-H. Kim, Z. Bian, A.F. McKenzie, N.D. Gerrard, K.J. Rae, P. Ivanov, R.J.E. Taylor, R.A. Hogg, D.T.D. Childs, Monolithic all-semiconductor PCSELs emitting at 1.3 μm, in: 27th International Semiconductor Laser Conference, WP3.4, Potsdam, Germany, October 2021.
[14] P.D. Dapkus, C.Y. Chi, S.J. Choi, H.J. Chu, M. Dreiske, R. Li, Y. Lin, Y. Nakajima, D. Ren, R. Stevenson, M. Yao, T.W. Yeh, H. Zhao, Selective area epitaxy by metalorganic chemical vapor deposition – a tool for photonic integration and novel nanostructure integration, Prog. Quant. Electron. 75 (2021), 100304.
[15] J.J. Coleman, R.M. Lammert, M.L. Osowski, A.M. Jones, Progress in InGaAs-GaAs selective area MOCVD towards photonic integrated circuits, IEEE J. Select. Topics Quant. Electron. 3 (3) (1997) 874.
[16] T.M. Cockerill, R.M. Lammert, D.V. Forbes, M.L. Osowski, J.J. Colman, Twelve-channel strained-layer InGaAs-GaAs-AlGaAs buried heterostructure quantum well laser array for WDM applications by selective-area MOCVD, IEEE Photon. Technol. 6 (7) (1994) 786.
[17] C. Besancon, D. Néel, D. Make, J.M. Ramirez, G. Cerulo, N. Vaissiere, D. Bitauld, F. Pommereau, F. Fournel, G. Dupré, H. Mehdi, F. Bassani, J. Decobert, AlGaInAs multi-quantum well lasers in silicon-on-insulator photonic integrated circuits based on InP-seed-bonding and epitaxial regrowth, Appl. Sci. 12 (2022) 263.
[18] T.M. Cockerill, D.V. Forbes, J.A. Dantzig, J.J. Coleman, Strained-layer InGaAs-GaAs-AlGaAs buried-heterostructure quantum-well lasers by three-step selective-area metalorganic chemical vapor deposition, IEEE J. Quant. Electron. 30 (2) (1994) 441.
[19] M. Aoki, M. Suzuki, H. Sano, T. Kawano, T. Iddo, T. Taniwatarai, K. Uomi, A. Takai, InGaAs/InGaAsP MQW electroabsorption modulator integrated with a DFB laser fabricated by bang-gap energy control selective area MOCVD, IEEE J. Quant. Electron. 29 (6) (1993) 2088.
[20] J. Decobert, G. Binet, A.D.B. Maia, P.-Y. Lagrée, C. Kazmierski, AlGaInAs MOVPE selective area growth for integrated circuits, Adv. Opt, Technol. 4 (2) (2015) 167.
[21] V. Shamakhov, D. Nikolaev, S. Slipchenko, E. Fomin, A. Smimov, I. Eliseyev, N. Pikhtin, P. Kop'ev, Surface nanostructuring during selective area epitaxy of heterostructures with InGaAs QWs in the ultra-wide windows, Nanomaterials 11 (2021) 11.
[22] T.M. Cockerill, D.V. Forbes, H. Han, B.A. Turkot, J.A. Dantzig, I.M. Robertson, J. J. Colman, Wavelength tuning in strained layer InGaAs-GaAs-AlGaAs quantum well laser by selective-area MOCVD, J. Electron. Mater. 23 (2) (1994) 115.
[23] O.K. Kwon, Y.A. Leek, C.W. Lee, K.S. Kim, H.M. Park, E.S. Nam, Simple technique for evaluating dimensional and compositional changed in selective-area-grown MQW laser diodes, Optics Express 22 (19) (2014) 23694.
[24] N. Dupuis, J. Décobert, P.-Y. Lagrée, N. Lagay, F. Poingt, C. Kazmierski, A. Ramdane, A. Ougazaden, Mask pattern interference in AlGaInAs selective area metal-organic vapor-phase epitaxy: experimental and modelling analysis, J. Appl. Phys. 103 (2008), 113113.
[25] J. Décobert, R. Guillamet, C. Mocuta, G. Carbone, H. Guerault, Structural characterisation of selectively grown multilayers with new high angular resolution and sub-millimeter spot-size x-ray diffractometer, J. Cryst. Growth 370 (2013) 154.
[26] A.M. Jones, M.L. Osowski, R.M. Lammert, J.A. Dantzig, J.J. Colman, Growth, characterisation, and modelling of ternary InGaAs-GaAs quantum wells by selective-area metalorganic chemical vapour deposition, J. Electron Mater. 26 (11) (1995) 1631.
[27] E.J. Thrush, J.P. Stagg, M.A. Gibbon, R.E. Mallard, B. Hamilton, J.M. Jowett, E. M. Allen, Selective and non-planar epitaxy of InP/GaInAs(P) by MOCVD, Mater. Sci. Eng. 21 (2) (1993) 130.
[28] M. Gibbon, J.P. Stagg, C.G. Cureton, E.J. Thrush, C.J. Jones, R.E. Mallard, R. E. Pritchard, N. Collis, A. Chew, Selective-area low-pressure MOCVD of GaInAsP and related materials on planar InP substrates, Semicond. Sci. Technol. 8 (1993) 998.
[29] T.M. Cockerill, D.V. Forbes, H. Han, J.J. Coleman, Monolithic Integration of a strained-layer InGaAs-GaAs-AlGaAs quantum-well laser with a passive waveguide by selective-area MOCVD, IEEE Photon. Technol. Lett. 4 (4) (1993) 448.